Signaling from the RNA sensor RIG-I is regulated by ufmylation

Daltry L. Snider[1], Moonhee Park[1], Kristen A. Murphy[1], Dia C. Beachboard[1, a], Stacy M. Horner[1,2,*]

[1] Department of Molecular Genetics & Microbiology, Duke University Medical Center, Durham, NC 27710, USA

[2] Department of Medicine, Duke University Medical Center Durham, NC 27710, USA

[a] Current address: DeSales University, Center Valley, Pennsylvania, 18034

* Correspondence: stacy.horner@duke.edu

Stacy M. Horner, Ph.D.

Duke University Medical Center

213 Research Dr., Box 3053 DUMC

Durham, NC USA 27710

Keywords

Retinoic acid-inducible gene I, RLR signaling, ubiquitin-like modifications, mitochondrial-associated ER membranes

Abstract

The RNA binding protein RIG-I is a key initiator of the antiviral innate immune response. The signaling that mediates the antiviral response downstream of RIG-I is transduced through the adaptor protein MAVS and results in the induction of type I and III interferons (IFN). This signal transduction occurs at endoplasmic reticulum (ER)-mitochondrial contact sites, to which RIG-I and other signaling proteins are recruited following their activation. RIG-I signaling is highly regulated to prevent aberrant activation of this pathway and dysregulated induction of IFN. Previously, we identified UFL1, the E3 ligase of the ubiquitin-like modifier conjugation system called ufmylation, UFL1, as one of the proteins recruited to membranes at ER-mitochondrial contact sites in response to RIG-I activation. Here, we show that UFL1, as well as the process of ufmylation, promote IFN induction in response to RIG-I activation. We find that following RNA virus infection, UFL1 is recruited to the membrane targeting protein 14-3-3ε, and that this complex is then recruited to activated RIG-I to promote downstream innate immune signaling. Importantly, loss of ufmylation prevents 14-3-3ε interaction with RIG-I, which abrogates the interaction of RIG-I with MAVS and thus downstream signal transduction that induces IFN. Our results define ufmylation as an integral regulatory component of the RIG-I signaling pathway and as a post-translational control for IFN induction.

Significance

The viral RNA sensor RIG-I initiates the antiviral innate immune response by activating a signaling cascade that induces interferon. Activation of the RIG-I signaling pathway is highly regulated to quickly mount a protective immune response while preventing dysregulation that can lead to excessive inflammation or autoimmune disorders. Here, we characterize one such mechanism of regulation. We describe that UFL1, an E3 ligase for the ubiquitin-like modifier conjugation system called ufmylation, is important to promote RIG-I signaling. Using molecular approaches, we show that ufmylation promotes RIG-I interaction with the membrane targeting protein 14-3-3ε. As such, ufmylation positively regulates RIG-I recruitment to its signaling adaptor proteins MAVS for induction of interferon in response to RNA virus infection.

Abstract

The RNA binding protein RIG-I is a key initiator of the antiviral innate immune response. The signaling that mediates the antiviral response downstream of RIG-I is transduced through the adaptor protein MAVS and results in the induction of type I and III interferons (IFN). This signal transduction occurs at endoplasmic reticulum (ER)-mitochondrial contact sites, to which RIG-I and other signaling proteins are recruited following their activation. RIG-I signaling is highly regulated to prevent aberrant activation of this pathway and dysregulated induction of IFN. Previously, we identified UFL1, the E3 ligase of the ubiquitin-like modifier conjugation system called ufmylation, UFL1, as one of the proteins recruited to membranes at ER-mitochondrial contact sites in response to RIG-I activation. Here, we show that UFL1, as well as the process of ufmylation, promote IFN induction in response to RIG-I activation. We find that following RNA virus infection, UFL1 is recruited to the membrane targeting protein 14-3-3ε, and that this complex is then recruited to activated RIG-I to promote downstream innate immune signaling. Importantly, loss of ufmylation prevents 14-3-3ε interaction with RIG-I, which abrogates the interaction of RIG-I with MAVS and thus downstream signal transduction that induces IFN. Our results define ufmylation as an integral regulatory component of the RIG-I signaling pathway and as a post-translational control for IFN induction.

Significance Statement

The viral RNA sensor RIG-I initiates the antiviral innate immune response by activating a signaling cascade that induces interferon. Activation of the RIG-I signaling pathway is highly regulated to quickly mount a protective immune response while preventing dysregulation that can lead to excessive inflammation or autoimmune disorders. Here, we characterize one such mechanism of regulation. We describe that UFL1, an E3 ligase for the ubiquitin-like modifier conjugation system called ufmylation, is important to promote RIG-I signaling. Using molecular approaches, we show that ufmylation promotes RIG-I interaction with the membrane targeting protein 14-3-3ε. As such, ufmylation positively regulates RIG-I recruitment to its signaling adaptor proteins MAVS for induction of interferon in response to RNA virus infection.

Introduction

Detection of RNA virus infection is initiated by cellular sensors such as RIG-I. RIG-I is a pattern recognition receptor that detects unique features of viral RNA that are generally

97 absent in cellular RNA, referred to as pathogen-associated molecular patterns (PAMPs)
98 (1). Sensing of viral RNA PAMPs triggers RIG-I activation and induces a downstream
99 signaling cascade that ultimately results in transcriptional induction of type I and type III
100 interferons (IFN) and the antiviral response (2, 3). The RIG-I signaling cascade is carefully
101 regulated by multiple mechanisms, including post-translational modifications that
102 influence specific protein-protein interactions that can result in changes in protein
103 localization to mediated signaling (3, 4). For example, following sensing of RNA PAMPs,
104 RIG-I undergoes K63-linked polyubiquitination in order to transition to its fully active
105 conformation, which promotes its interaction with the molecular trafficking protein 14-3-3ε
106 (5–8). 14-3-3ε facilitates the recruitment of activated RIG-I from the cytosol to intracellular
107 membranes where it interacts with MAVS (7, 9, 10), which assembles other RIG-I pathway
108 members to transduce the signals that induce IFN (7, 11). Importantly, many RNA viruses,
109 including influenza A virus and some flaviviruses (dengue virus, Zika virus, and West Nile
110 virus), prevent the interaction of RIG-I with 14-3-3ε to limit IFN induction and evade the
111 antiviral response (9, 10, 12).
112
113 In addition to RIG-I, a number of signaling proteins must be recruited to MAVS in order to
114 propagate downstream IFN induction. Previously, we identified proteins that move to
115 MAVS signaling sites at mitochondrial-associated endoplasmic reticulum (ER)
116 membranes (MAM) during RNA virus infection (13, 14). These proteins likely aid in spatial
117 organization of RIG-I pathway proteins during viral infection and include the GTPase
118 RAB1B, which plays a role in recruiting TRAF3 to MAVS (15). In addition to RAB1B, we
119 identified other proteins recruited to the MAM upon RIG-I signaling activation, one of which
120 was UFL1 (referred to in our previous publication as KIAA0776) (14). UFL1 is an E3 ligase
121 for UFM1, which is a ubiquitin-like modification of 85 amino acids. The process of
122 ufmylation conjugates UFM1 covalently to lysine residues of target proteins through a
123 process called ufmylation, which is similar to ubiquitination in that it also uses an E1, E2,
124 and E3 ligase conjugation system (UBA5, UFC1, and UFL1; see Figure 2D). UFM1 is
125 removed by the UFSP2 protease (16–20). The consequence of UFM1 addition to proteins
126 is not fully understood, but the literature supports the idea that it can promote protein-
127 protein interactions to regulate a number of biological processes (21–31). Here, we
128 uncover a role for ufmylation in RIG-I activation. We found that the cellular proteins that
129 catalyze ufmylation all promote RIG-I-mediated induction of IFN. Interestingly, we found
130 that UFL1 interacts with both RIG-I and the molecular trafficking protein 14-3-3ε following

131 RNA virus infection. Further, similar to RIG-I, UFL1 is recruited to intracellular membranes
132 following RNA virus infection. Importantly, loss of ufmylation prevents the interaction of
133 14-3-3ε with RIG-I, which results in decreased MAVS activation and IFN induction in
134 response to RNA virus infection. Thus, ufmylation can regulate RIG-I activation and
135 downstream signaling of the intracellular innate immune system.
136
137 **Results**
138
139 **The ufmylation activity of UFL1 promotes RIG-I signaling.** Having found that the E3
140 ligase of ufmylation UFL1 is recruited to MAVS signaling sites at the MAM in response to
141 RIG-I signaling (14), we wanted to determine if UFL1 regulates RIG-I signaling. To test
142 this, we measured induction of the IFN-β promoter following UFL1 overexpression using
143 an IFN-β promoter luciferase reporter assay (32) and found that UFL1 increased activation
144 of the IFN-β promoter, similar to that of RIG-I expression, in a dose-dependent fashion in
145 response to infection with Sendai virus (SenV) (Figure 1A). SenV is a murine
146 paramyxovirus that specifically activates RIG-I (33). In support of UFL1 enhancing RIG-I
147 signaling specifically, exogenous expression of UFL1 also increased IFN-β promoter
148 activity in response to transfection of 293T cells with a known RIG-I immunostimulatory
149 RNA from hepatitis C virus (PAMP; Figure 1B) (34). However, UFL1 overexpression in
150 293T cells did not lead to increased induction of IFN-stimulated genes (ISG), such as
151 *ISG56* or *ISG15,* in response to exogenous IFN-β treatment, indicating that UFL1 primarily
152 regulates IFN induction and not the IFN response (Figure 1C). Next, we depleted UFL1
153 by siRNA in two different cell types and measured SenV-induced activation of the RIG-I
154 pathway. Depletion of UFL1 in 293T cells resulted in decreased phosphorylation of IRF3,
155 a transcription factor for both type I and III IFNs, while exogenous expression of an siRNA-
156 resistant UFL1 restored SenV-mediated IRF3 phosphorylation (Figure 1D). Depletion of
157 UFL1 in primary neonatal human dermal fibroblasts (NHDFs) also reduced the SenV-
158 mediated induction of both *IFNB1* and *IFNL1* transcripts, as measured by RT-qPCR
159 (Figure 1E), as well as the production of IFN-β protein, as measured by an enzyme-linked
160 immunosorbent assay (ELISA) (Figure 1F).
161
162 To define the domains of UFL1 that regulate RIG-I signaling, we expressed a series of
163 previously described UFL1 truncation mutants (diagrammed in Figure 1H) and measured
164 SenV-mediated activation of the IFN-β promoter in a luciferase reporter assay (16). The

165 ability of UFL1 to transfer UFM1 to a target protein has been suggested to require the first
166 212 amino acids of the protein, as this domain interacts with the E2 ligase for ufmylation,
167 UFC1 (16). The wild-type (WT) UFL1 (aa 1-794), as well as the C-terminal deleted mutants
168 of UFL1, aa 1-212 and aa 1-452, which all have reported ufmylation activity (16),
169 stimulated SenV-medicated induction of the IFN-β promoter (Figure 1G). Interestingly, the
170 N-terminal deleted mutant of UFL1 aa 213-794, that does not have reported ufmylation
171 activity, also induced signaling, while the N-terminal deleted UFL1 mutant aa 453-794 did
172 not (Figure 1G). However, our analysis of global UFM1 conjugates by these UFL1
173 constructs revealed that while UFL1 WT, aa 1-212, and aa 1-452 all retain full ufmylation
174 activity, aa 213-794 of UFL1 retain approximately 40% ufmylation activity, while aa 453-
175 794 of UFL1 retain only about 20% activity (Figure 1H; Figure S1). Thus, taken together,
176 this reveals that the ufmylation activity of UFL1 is required to promote RIG-I signaling that
177 results in induction of IFN.
178
179 **The ufmylation machinery proteins positively regulate RIG-I signaling**. Having
180 determined that the ufmylation activity of UFL1 is important for its role in RIG-I signaling,
181 we hypothesized that UFM1 and the proteins required for UFM1 conjugation would also
182 be required to promote this signaling. Similar to our results with UFL1, overexpression of
183 UFM1 increased SenV-mediated activation of the IFN-β promoter in a dose-dependent
184 fashion (Figure 2A). Conversely, the activation of the IFN-β promoter in response to SenV
185 was significantly abrogated in 293T cells in which UFM1 was deleted by CRISPR/Cas9,
186 as compared to WT 293T cells (Figure 2B). Importantly, this signaling was restored upon
187 exogenous expression of UFM1 (Figure 2B). The absence of UFM1 expression also
188 prevented the induction of IFN-β protein in response to SenV infection, as measured by
189 ELISA (Figure 2C). The process of ufmylation has 5 steps (Figure 2D). First, UFM1 is
190 processed to expose the terminal glycine residue. Then, this mature UFM1 is added to the
191 target protein by the actions of UBA5, which acts as an E1 ligase for UFM1; UFC1, the E2
192 ligase; and UFL1, the E3 ligase (19). Finally, the UFSP2 protease removes UFM1, which
193 enables recycling of mature UFM1 (18). We found that exogenous expression of each of
194 the proteins involved in UFM1 conjugation, including the UFSP2 protease, positively
195 regulated SenV-mediated induction of the IFN-β promoter (Figure 2E). These results
196 reveal that the proteins that catalyze ufmylation and the UFM1 modification itself promote
197 RIG-I signaling.
198

199 **UFM1 is required for the RIG-I-driven transcriptional response.** After establishing that
200 ufmylation promotes RIG-I activation, and in turn IFN expression, we next broadly
201 measured the impact of ufmylation upon the transcriptional response to RIG-I signaling.
202 Using RNA-sequencing, we analyzed gene expression in either WT or UFM1 KO 293T
203 cells, following mock or SenV infection (Table S1.1; Table S1.2). Gene set enrichment
204 analysis (Table S2.1; Table S2.2) of the transcripts significantly reduced (adjusted P<0.01)
205 by UFM1 KO in the absence of viral infection revealed previously described pathways
206 regulated by ufmylation such as cytosolic ribosomes, ribosome assembly, and
207 hematopoiesis (Figure S2A; Table S2.1) (21, 28, 29, 35). Following viral infection, the top
208 10 gene categories negatively impacted by UFM1 KO, with a darker red color indicating
209 more downregulation, were all related to the antiviral response, such as response to type
210 I IFN and defense against virus (Figure 3A; Table S2.2). Indeed, of the top 50 most
211 downregulated pathways impacted by UFM1 KO during infection, the majority were related
212 to innate immune signaling or viral replication (Table S2.2), while upregulated gene
213 categories were more diverse (Table S2.3; Table S2.4). Of the genes differentially
214 expressed during UFM1 KO in response to SenV (adjusted P<0.01), the majority are
215 downregulated (Figure 3B). Indeed, these downregulated genes included *IFNB1* and
216 *IFNL1*, as well as other known ISGs (in red) (36) (Figure 3B; Figure 3C). These data are
217 consistent with a model in which ufmylation-mediated regulation of IFN induction has
218 broad consequences on genes induced by the IFN response.
219
220 **UFL1 is recruited to intracellular membranes and interacts with 14-3-3ε and RIG-I**
221 **during RNA virus infection.** Following the binding of RIG-I to non-self RNA, it interacts
222 with several host proteins to facilitate its activation, localization to the MAM, and interaction
223 with MAVS. These proteins include the E3 ligases for K63-linked ubiquitin TRIM25 and
224 Riplet (5, 6, 37), as well as the molecular trafficking protein 14-3-3ε. In particular, 14-3-3ε
225 is required for RIG-I recruitment from the cytosol to MAVS signaling sites at intracellular
226 membranes (5–7, 13); however, the mechanism underlying how 14-3-3ε selects RIG-I as
227 cargo has yet to be elucidated. Using a subcellular membrane fractionation assay (38),
228 we confirmed that UFL1 increases its association with intracellular membranes in
229 response to SenV, similar to RIG-I (Figure 4A; compare fraction #1, which has Cox-I and
230 no GAPDH, with fractions #6-8, which are enriched for the cytosolic protein GAPDH) (7,
231 12). This finding is consistent with our previous report that UFL1 is recruited to the MAM
232 in response to either SenV or hepatitis C virus replication (14), suggesting that UFL1

233 recruitment occurs prior to MAVS activation, as MAVS is cleaved by the HCV NS3-NS4A
234 protease (39–42). As the recruitment of RIG-I to intracellular membranes is known to
235 require 14-3-3ε, and, as both UFL1 and UFM1 have been shown to interact with 14-3-3ε
236 (16), we hypothesized that UFL1 may interact with 14-3-3ε to promote the IFN induction
237 that we had observed in response to RNA virus infection. Thus, we first determined if the
238 interaction of UFL1 with 14-3-3ε is increased in response to RIG-I activation by SenV by
239 performing co-immunoprecipitation. We found that Myc-14-3-3ε did co-immunoprecipitate
240 with Flag-UFL1, as reported previously (16), and that this interaction was increased by
241 SenV (Figure 4B). Interestingly, the interaction of UFL1 with RIG-I also increased following
242 SenV, both upon over-expression and at the level of the endogenous proteins (Figure 4C;
243 Figure 4D). As RIG-I undergoes a series of modifications to become fully active (1, 4), we
244 next used a panel of RIG-I mutants to define which stage of RIG-I activation promotes
245 interaction with UFL1. These mutations prevent the distinct steps of RIG-I activation such
246 as RIG-I binding to RNA (K888/907A), interacting with TRIM25 (T55I), or ubiquitination by
247 Riplet and TRIM25 (K172/788R) (5, 43, 44). The interaction of UFL1 with RIG-I was
248 significantly impaired by each of these mutations, suggesting that UFL1 regulates RIG-I
249 function after it binds RNA and becomes ubiquitinated (Figure 4E). As this is the same
250 step of activation at which 14-3-3ε binds to RIG-I to promote its translocation to
251 intracellular membranes (7), this suggests that RNA virus infection increases the
252 interaction of 14-3-3ε with UFL1, which then interacts with activated, K63-ubiquitinated
253 RIG-I.
254
255 **UFL1 interaction with RIG-I requires 14-3-3ε and UFM1.** Having determined that UFL1
256 interacts with both activated RIG-I and 14-3-3ε following RNA virus infection, we next
257 defined the dynamics of this complex formation by testing two distinct models. In the first
258 model, UFL1 would interact first with activated RIG-I, induce its ufmylation, and then the
259 UFL1-RIG-I complex would interact with 14-3-3ε. In this model, depletion of 14-3-3ε or
260 loss of UFM1 would not be expected to change the interaction of UFL1 with RIG-I. In the
261 second model, UFL1 would interact first with 14-3-3ε and induces its ufmylation, or that of
262 another associated protein, and then the UFL1-14-3-3ε complex would interact with
263 activated RIG-I. In this second model, depletion of 14-3-3ε would be expected to prevent
264 UFL1 interaction with RIG-I, and loss of ufmylation would limit UFL1 interaction with RIG-
265 I but would not affect UFL1 interaction with 14-3-3ε. To elucidate these possibilities, first,

266 we used co-immunoprecipitation to measure the interaction of exogenously expressed
267 Flag-UFL1 and HA-RIG-I in SenV-infected 293T lysates that had been depleted of 14-3-
268 3ε or CTRL by siRNA. This revealed that formation of the SenV-activated RIG-I-UFL1
269 complex requires 14-3-3ε (Figure 5A). Next, we tested if ufmylation was required for
270 formation of the SenV-activated RIG-I-UFL1 complex by measuring this interaction in WT
271 or UFM1 KO 293T cells. We found that UFM1 was required for SenV-activated RIG-I-
272 UFL1 complex (Figure 5B). The results of these two experiments reveal that both 14-3-3ε
273 and UFM1 are required for UFL1 to interact with RIG-I, supporting the second model of
274 complex formation in which UFL1 interacts first with 14-3-3ε and catalyzes its ufmylation,
275 and then this complex associates with RIG-I. In support of this, we found that UFM1 was
276 not required for UFL1 to interact with 14-3-3ε (Figure 5C). Together, these data indicate
277 that ufmylation promotes the interaction of UFL1 with 14-3-3ε and activated RIG-I.
278
279 **Ufmylation promotes RIG-I interaction with 14-3-3ε for MAVS activation.** Having
280 found that that UFL1 requires 14-3-3ε to interact with activated RIG-I, we next tested if
281 UFL1 is required for the interaction of 14-3-3ε with RIG-I, which is essential for activated
282 RIG-I to translocate from the cytosol to intracellular membranes for interaction with MAVS
283 (7). We performed a co-immunoprecipitation of Flag-RIG-I and Myc-14-3-3ε from 293T
284 cells and found that this SenV-mediated interaction was significantly decreased upon
285 UFL1 depletion (Figure 6A). In addition, loss of UFM1 expression also decreased the
286 SenV-induced interaction of RIG-I with 14-3-3ε (Figure 6B). Importantly, we also found
287 that UFM1 is required for the SenV-induced interaction of RIG-I with MAVS (Figure 6C)
288 and MAVS higher-order oligomerization, which is a hallmark of MAVS activation (45, 46)
289 (Figure 6D). In summary, these data reveal that UFL1 and UFM1 are required for the RIG-
290 I interaction with 14-3-3ε, for interaction with MAVS, and for MAVS activation by
291 oligomerization.
292
293 **Discussion**
294
295 Regulation of RIG-I activation and downstream signaling is essential for proper induction
296 and termination of IFN. Here, we show that both UFL1 and the process of ufmylation
297 promote RIG-I pathway signaling that leads to IFN induction, uncovering an important step
298 in the activation of the RIG-I pathway. RIG-I activation occurs upon RNA binding. Then,

299 RIG-I undergoes ATP hydrolysis. and interaction with K63-linked polyubiquitin chains,
300 both covalently and non-covalently (5, 44, 47), which promotes formation of a RIG-I
301 tetramer (48). This polyubiquitinated, activated RIG-I oligomer then interacts with the
302 membrane trafficking protein 14-3-3ε for translocation to MAVS at ER-mitochondrial
303 contact sites (7). We found that UFL1 is recruited to 14-3-3ε following RNA virus infection
304 and that ufmylation facilitates the interaction between 14-3-3ε and activated RIG-I.
305 Importantly, this results in increased interaction of RIG-I with MAVS and MAVS
306 oligomerization, ultimately promoting the downstream signal transduction which produces
307 IFN.
308
309 Ufmylation is emerging as a post-translational modification that regulates diverse
310 biological processes, including DNA repair, ER homeostasis, and even the replication of
311 hepatitis A virus (21, 22, 24, 27, 28, 30, 35, 49). In these cases, UFL1, along with the other
312 members of the ufmylation cascade, induce ufmylation of a target protein important for
313 regulating these processes. For example, both MRE11 and histone H4 are ufmylated by
314 UFL1 in the nucleus in response to DNA damage resulting in activation the key DNA repair
315 kinase ATM (22, 24). UFL1 can also act at the ER, where it plays a role in ER protein
316 quality control, where it ufmylates specific proteins, including ribosomal proteins RPL26,
317 to induce lysosomal degradation of stalled peptides and/or the ER and prevent the
318 unfolded protein response (27, 28, 49, 50). Interestingly, hepatitis A virus translation,
319 which occurs in association with the ER, also requires ufmylation of RPL26 (30).
320 Therefore, ufmylation can regulate several aspects of translation. It is possible that
321 ufmylation regulates translation of certain mRNAs important for RIG-I signaling and
322 subsequent IFN induction. However, we identified a role for ufmylation in regulating the
323 interaction of RIG-I with 14-3-3ε, one of the earliest known steps of RIG-I signaling,
324 strongly supporting a mechanism in which following RIG-I activation, ufmylation is
325 controlling this specific protein-protein interaction. The mechanisms by which the process
326 of UFM1 addition regulates interactions between proteins or alters other aspects of protein
327 function are largely unknown. Indeed, we found that UFSP2, the protease that removes
328 UFM1 from proteins (18), promoted SenV-mediated IFN induction (Figure 2D), suggesting
329 that we do not yet have a full grasp on the ufmylation process. It is possible that the
330 dynamic process of ufmylation or the enhanced formation of mature UFM1 following
331 deconjugation from targets or promote RIG-I signaling independent of deconjugation
332 activity. Indeed, in support of this idea, others have shown that UFSP2 in myeloid cells is

333 required for influenza virus resistance in mice (31). It is also possible that UFSP2 acts on
334 other members of the RIG-I pathway to alter their function. Future studies to define how
335 the process of ufmylation regulates this and other aspects of the antiviral innate immune
336 response will be of great interest as they may shed light broadly on how ufmylation
337 regulates diverse cell biological processes that alter cellular signaling.
338
339 The mechanisms underlying how cytoplasmic UFL1 is recruited to its protein targets that
340 reside in different subcellular compartments are not fully known. For example, we found
341 that RIG-I activation induces UFL1 translocation to intracellular membranes (Figure 3A),
342 and while we know that UFL1 is recruited to the MAM during infection, the mechanism by
343 which UFL1 becomes membrane-associated remains unknown (14). DDRGK1 (UFBP1)
344 may facilitate UFL1 targeting to the MAM, as DDRGK1 is localized to mitochondrial-ER
345 contact sites (16, 51) and in some cases it is required for UFL1 recruitment to membranes
346 (27, 28). Thus, both DDRGK1 and mitochondrial-ER contact sites could function as a
347 regulatory hub that aids in the recruitment of UFL1 and RIG-I pathway signaling proteins.
348 Interestingly, RAB1B, a GTPase that we found is recruited to the MAM and important for
349 RIG-I signaling (14, 15) is ufmylated (52, 53), which reveals that ufmylation likely regulates
350 a number of RIG-I pathway signaling proteins. As UFL1 contains no functional domains
351 common to other E3 ligases that might allow one to predict how its targets are selected
352 (16, 54, 55), defining the signals and features that control UFL1 localization, as well as
353 the target proteins ufmylated in response to RIG-I activation, will undoubtedly reveal clues
354 into how the process of ufmylation is activated and how specific targets are selected.
355
356 Our work revealed that 14-3-3ε required ufmylation to interact with activated RIG-I. The
357 details underlying how 14-3-3ε interacts with activated RIG-I have not been fully
358 elucidated, as it does not occur through the known phosphorylated amino acids on RIG-I,
359 the typical recruitment signal of the 14-3-3 family of proteins (7, 56, 57). Interestingly,
360 others have shown that 14-3-3ε interacts with UFM1 and other members of the ufmylation
361 pathway (16). Thus, taken together with our results, this suggests that ufmylation of 14-3-
362 3ε or a 14-3-3ε-associated protein promotes the interaction between activated RIG-I and
363 14-3-3ε. In fact, a number of 14-3-3 family proteins are post-translationally modified by
364 phosphorylation, acetylation, and oxidation (58). Therefore, post-translational modification
365 of 14-3-3ε by ufmylation could broadly define how cargo proteins, including RIG-I, are
366 selected. Indeed, this mechanism could be shared with other RNA virus sensing

367 pathways, such as the RIG-I-like-receptor MDA5, which also interacts with a 14-3-3
368 protein, 14-3-3η, by an unknown mechanism (59). Thus, ufmylation may broadly influence
369 how 14-3-3 proteins or other host proteins interact with each other to regulate the
370 intracellular innate immune response.
371
372 Overall, this work lays the groundwork for future studies to define how ufmylation of
373 antiviral innate immune signaling proteins regulates their function and how specific
374 signaling pathways are differentially activated through ufmylation. In addition, our work
375 adds ufmylation to the growing list of ubiquitin-like and other modifications that regulate
376 the intracellular innate immune response, including ISGylation, SUMOylation, FATylation,
377 acetylation, phosphorylation, and others (4, 60, 61) broadening our understanding of how
378 RIG-I signaling is activated and rapidly controlled by post-translational modifications in
379 response to infection, leading to greater knowledge of the exquisite regulation of these
380 pathways.
381
382 **Materials and Methods**
383
384 **Cell lines, viruses, and treatments.** Neonatal human dermal fibroblast (NHDF) cells and
385 embryonic kidney 293T cells were grown in Dulbecco's modification of Eagle's medium
386 (DMEM; Mediatech) supplemented with 10% fetal bovine serum (Thermo Fisher
387 Scientific), 1X minimum essential medium non-essential amino acids (Thermo Fisher
388 Scientific), and 25 mM HEPES (Thermo Fisher Scientific) (cDMEM). 293T (CRL-3216)
389 were obtained from American Type Culture Collection (ATCC), NHDF cells (CC-2509)
390 were obtained from Lonza. All cell lines were verified as mycoplasma free by the LookOut
391 Mycoplasma PCR detection kit (Sigma). SenV Cantell strain was obtained from Charles
392 River Laboratories and used at 200 hemagglutination units/mL (HAU). SenV infections
393 were performed in serum-free media (30 minutes to 1 hour), after which complete media
394 was replenished. IFN-β (PBL Assay Science) was added to cells at a concentration of 50
395 units/mL in cDMEM for 18 hours.
396
397 **Plasmids.** The following plasmids have been previously described: pEF-TAK-Flag, pEF-
398 BOS-Flag-RIG-I (62), pIFN-β-luc (63), pCMV-Renilla (Promega), pX459 (Addgene
399 Plasmid #62988), pEF-BOS-Flag-RIG-I T55I (64), pEF-TAK-Myc-MAVS (32).
400 pLJM1_Flag-UFM1 was a gift from Dr. Craig McCormick at Dalhouise University. The

401 following plasmids were generated by insertion of PCR-amplified fragments into the NotI-
402 to-PmeI digested pEF-TAK-Flag using InFusion cloning (Clontech), all primers are
403 denoted in Table 1: pEF-TAK-Flag-UFL1 (GenBank: BC036379; GeneID: 23376), pEF-
404 TAK-Flag-UBA5 (NM_024818.6), pEF-TAK-Flag-UFC1 (NM_016406.4), pEF-TAK-Flag-
405 UFSP2 (NM_018359.5), pEF-TAK-Flag-UFL1 1-212, pEF-TAK-Flag-UFL1 1-452, pEF-
406 TAK-Flag-UFL1 213-794, and pEF-TAK-Flag-UFL1 453-794. Both pEF-TAK-Myc-14-3-3ε
407 and pEF-TAK-Myc-UFL1 were generated by insertion of PCR-amplified fragments into the
408 AgeI-NotI digested pEF-TAK-Myc (pEF-TAK-Myc-MAVS) by InFusion. The pEF-TAK-HA
409 vector was generated by PCR to replace Flag with HA, and pEF-TAK-HA-RIG-I was
410 generated by insertion of a PCR-amplified fragment into the NotI-AgeI digested pEF-TAK-
411 HA vector. The following plasmids were generated by site-directed mutagenesis (see
412 Table 1): pEF-TAK-Flag-UFL1^{siR}, pEF-BOS-Flag-RIG-I K888/907A, and pEF-BOS-Flag-
413 RIG-I K172/788R. To generate the CRISPR guide RNA plasmids px459-UFM1-E2 and
414 px459-UFM1-B, sgRNA oligonucleotides were annealed and inserted into the BbsI-
415 digested pX459 (30, 65). The plasmid sequences were verified by DNA sequencing and
416 oligonucleotide sequences are available upon request.
417
418 **Generation of RNA PAMP.** Annealed oligonucleotides containing the sequence of the
419 HCV 5'ppp poly-U/UC region (34) were *in vitro* transcribed using the MEGAshortscript T7
420 transcription kit (Ambion) followed by ethanol precipitation, with the resulting RNA
421 resuspended at 1 µg/µL.
422
423 **Transfection.** DNA transfections were performed using FuGENE6 (Promega) or TransIT-
424 LT1 (Mirus Bio). RNA PAMP transfections were done using the TransIT-mRNA
425 Transfection kit (Mirus Bio). The siRNA transfections were done using Lipofectamine
426 RNAiMax (Invitrogen). siRNAs directed against 14-3-3ε (Dharmacon-L-017302-02-0005),
427 UFL1 (Qiagen-SI04371318) or non-targeting AllStars negative control siRNA (Qiagen-
428 1027280) were transfected into 293T cells (25 pmol of siRNA; final concentration of 0.0125
429 µM) or NHDF cells (250 pmol of siRNA; final concentration of 0.25 µM). Media was
430 changed 4-24 hours post-transfection, and cells were incubated for 36-48 h post-
431 transfection prior to each experimental treatment. IFN-β-promoter luciferase assays were
432 performed as previously described at 18-24 hours post treatment and normalized to the
433 *Renilla* luciferase transfection control (33).
434

435 **ELISA.** IFN-β ELISAs were performed using Human IFN-beta DuoSet (R&D Systems)
436 with supernatants collected from cultured cells.
437
438 **Generation of KO cell lines.** UFM1 KO 293T cells were generated by CRISPR/Cas9,
439 using two guides targeting exon 2 and 3, similar to others, as we have done previously
440 (15, 30).
441
442 **RNA analysis.** Total cellular RNA was extracted using the RNeasy Plus mini kit (Qiagen).
443 RNA was then reverse transcribed using the iScript cDNA synthesis kit (BioRad), as per
444 the manufacturer's instructions. The resulting cDNA was diluted 1:3 in ddH2O. RT-qPCR
445 was performed in triplicate using the Power SYBR Green PCR master mix (Thermo-
446 Fisher) and QuantStudio 6 Flex RT-PCR system. Oligonucleotide sequences for qPCR
447 are available upon request.
448
449 **RNA-seq.** WT and UFM1 KO 293T cells were mock or SenV-infected (18 h) and
450 harvested in biological duplicate, followed by total RNA extraction via TRIzol reagent
451 (Thermo Fisher Scientific). Sequencing libraries were prepared using the KAPA Stranded
452 mRNA-Seq Kit (Roche) and sequenced on an Illumina Novaseq 6000 with 50 bp paired-
453 end reads (>20 million reads per sample) in an S1 flow cell by the Duke University Center
454 for Genomic and Computational Biology.
455 RNA-seq data was processed using the TrimGalore toolkit (66) which employs Cutadapt
456 (67) to trim low-quality bases and Illumina sequencing adapters from the 3' end of the
457 reads. Only reads that were 20nt or longer after trimming were kept for further analysis.
458 Reads were mapped to the GRCh38v93 version of the human genome and transcriptome
459 (68) using the STAR RNA-seq alignment tool (69). Reads were kept for subsequent
460 analysis if they mapped to a single genomic location. Gene counts were compiled using
461 the HTSeq tool (70). Only genes that had at least 10 reads in any given library were used
462 in subsequent analysis. Normalization and differential expression was carried out using
463 the DESeq2 (71) Bioconductor (72) package with the R statistical programming
464 environment. The false discovery rate was calculated to control for multiple hypothesis
465 testing. Gene set enrichment analysis (73) was performed to identify gene ontology terms
466 and pathways associated with altered gene expression for each of the comparisons
467 performed. All RNA-seq data are deposited in the GEO database under GSE186287.
468

469 **Immunoblotting.** Cells were lysed in a modified radioimmunoprecipitation assay (RIPA)
470 buffer (10 mM Tris [pH 7.5], 150 mM NaCl, 0.5% sodium deoxycholate, and 1% Triton X-
471 100) supplemented with protease inhibitor cocktail (Sigma) and Halt Phosphatase Inhibitor
472 (Thermo-Fisher), and post-nuclear lysates were isolated by centrifugation. Quantified
473 protein (between 5 -15 µg) was resolved by SDS/PAGE, transferred to nitrocellulose or
474 polyvinylidene difluoride (PVDF) membranes in a 25 mM Tris-192 mM glycine-0.01% SDS
475 buffer. Membranes were stained with Revert 700 total protein stain (LI-COR Biosciences)
476 and then blocked in 3% BSA in Tris-buffered saline containing 0.01% Tween-20 (TBS-T).
477 After washing with PBS-T or TBS-T (for phosphoproteins) buffer, following incubation with
478 primary antibodies, membranes were incubated with species-specific horseradish
479 peroxidase-conjugated antibodies (Jackson ImmunoResearch, 1:5000) or fluorescent
480 secondaries (LI-COR Biosciences), followed by treatment of the membrane with Clarity
481 Western ECL substrate (BioRad) and imaging on a LICOR Odyssey FC. The following
482 antibodies were used for immunoblotting: R-anti-SenV (MBL, 1:1000), M-anti-Tubulin
483 (Sigma, 1:1000), R-anti-GAPDH (Cell Signaling Technology, 1:1000), R-anti-p-IRF3 (Cell
484 Signaling Technology, 1:1000), R-anti-IRF3 (Cell Signaling Technology, 1:1000), R-anti-
485 UFL1 (Novus Biologicals, 1:1000), R-anti-UFM1 (Abcam, 1:1000), anti-RIG-I (M-
486 AdipoGen, R-Abcam, 1:1000), R-anti-14-3-3ε (Cell Signaling Technology, 1:1000), M-anti-
487 Flag M2 (Sigma, 1:1000), anti-Flag-HRP (Sigma, 1:1000-1:5000), R-anti-Flag (Sigma,
488 1:1000), anti-HA (M- and R-Sigma, 1:1000), and anti-Myc (M-Santa Cruz or R-Cell
489 Signaling Technology, 1:1000).
490
491 **Immunoprecipitation.** Cells were lysed in RIPA buffer with or without 10% glycerol.
492 Quantified protein (between 100-500 µg) was incubated with protein-specific, isotype
493 control antibody (R-Cell Signaling Technology or M-Thermo Fisher), or anti-Flag M2
494 magnetic beads (Sigma), in lysis buffer either at room temperature for 2 h or at 4ºC
495 overnight with head over tail rotation. The lysate/antibody mixture was then incubated with
496 Protein G Dynabeads (Invitrogen) for 1 h. Beads were washed 3X in PBS or RIPA buffer
497 and eluted in 2X Laemmli Buffer (BioRad) with or without 5% 2-Mercaptoethanol at 95ºC
498 for 5 min. Proteins were resolved by SDS/PAGE and immunoblotting, as above.
499
500 **Subcellular membrane fractionation.** Membrane fractionation was performed as
501 previously described (7, 12, 38, 74). Cells were lysed in hypotonic buffer (10 mM Tris-HCL
502 (pH 7.5), 10 mM KCl, and 5 mM $MgCl_2$ supplemented with protease inhibitor cocktail) for

503 10 minutes on ice followed by 20 passages through a 20-guage needle. Nuclei and
504 unbroken cells were removed by centrifugation at 1000xg for 5 min at 4ºC. The resulting
505 supernatants were mixed thoroughly with 72% sucrose and overlayed with 55% sucrose,
506 followed by 10% sucrose, all in low-salt buffer (2 nM EDTA, 20 nM HEPES (pH 8.0), 150
507 mM NaCl, 0.1% SDS, 1% Triton X-100). The gradients were subjected to centrifugation at
508 38,000 RPM in a Beckman SW41 Ti Rotor for 14 h at 4ºC. 1 mL fractions were collected
509 using a BioComp piston gradient fractionator and resulting fractions were divided in half
510 and mixed with 2 parts 100% methanol and precipitated overnight at -80ºC. Protein pellets
511 were collected by centrifugation and resuspended in 2X Laemmli buffer and heated for 5
512 min at 95ºC for immunoblot analysis. 10% pre-fractionated cells from each condition were
513 collected as the input.
514
515 **Semi-denaturing detergent agarose gel electrophoresis.** SDD-AGE was performed as
516 described (45, 46). Briefly, crude mitochondria (P5 fraction) were isolated from an equal
517 number of WT or UFM1 KO 293T cells that were mock or SenV infected (12 h),
518 resuspended in hypotonic buffer (10 mM Tris, pH 7.5, 10 mM KCl, 1.5 mM $MgCl_2$, and 0.5
519 mM EDTA). Resulting samples were split and 2X SDD-AGE sample buffer (0.5X TBE,
520 10% glycerol, 2% SDS, 0.2 mM Bromophenol Blue) buffer with or without 5% 2-
521 Mercaptoethanol was added, and samples were loaded onto a vertical 1.5% agarose gel.
522 Electrophoresis was performed with a constant voltage of 70 V at 4 °C in SDD-AGE
523 running buffer (1X TBE and 0.1% SDS). Gels were transferred onto a nitrocellulose
524 membrane overnight on ice at 25 V. Membranes were fixed in 0.25% glutaraldehyde in
525 PBS and immunoblotting was performed as usual. 15% of the SDD-AGE samples were
526 reserved for input.
527
528 **Quantification of immunoblots.** Immunoblots imaged using the LICOR Odyssey FC
529 were quantified by ImageStudio software, and raw values were normalized to relevant
530 controls for each antibody. Phosphoprotein values were normalized to Tubulin and
531 displayed as the percentage of signal from WT. Relative membrane association of UFL1
532 was quantified as the ratio of UFL1 to Cox-1 in fraction 1 normalized to total protein levels
533 of UFL1 in the input and displayed as the percentage of UFL1 membrane association
534 normalized to mock values.
535

Statistical analysis. Student's unpaired t-test, one-way ANOVA, or two-way ANOVA were implemented for statistical analysis of the data followed by appropriate post-hoc test (as indicated) using GraphPad Prism software. Graphed values are presented as mean ± SD or SEM (n = 3 or as indicated); *$p \leq 0.05$, **$p \leq 0.01$, and ***$p \leq 0.001$.

Acknowledgments

We thank colleagues who provided reagents (see Methods), the Duke Functional Genomics Core Facility, the Duke University Center for Genomic and Computational Biology, the Duke Genomic Analysis and Bioinformatics Shared Resource and Dr. Wei Chen for performing RNA-seq analysis, Dr. Madhuvanthi Vijayan and Boyoung Michelle Kim for generation and initial characterization of plasmids, Dr. Matthew Thompson for input in RNA-seq sample preparation and data processing, and Horner lab members for useful discussion. This work was supported by funds from Burroughs Wellcome Fund, National Institutes of Health: R21AI144380, R01AI155512, T32-CA009111, and an American Cancer Society Postdoctoral fellowship 131321-PF-17-188-01-MPC.

Author Contributions: Conceptualization: D.L.S., D.C.B., and S.M.H.; Investigation: D.L.S, D.C.B., and M.P.; Formal analysis: D.L.S., D.C.B., K.A.M., and S.M.H.; Writing – original draft: D.L.S. and S.M.H.; Writing – review and editing: D.C.B., D.L.S., and S.M.H. All authors read the manuscript and provided comments. Funding acquisition: S.M.H.

Competing Interest Statement: The authors declare that they have no conflicts of interest with the contents of this article. The content is solely the responsibility of the authors and does not necessarily represent the official views of the National Institutes of Health.

563 **Figure Legends**

564 **Figure 1. The ufmylation activity of UFL1 promotes RIG-I signaling.**

565 A) IFN-β-promoter reporter luciferase expression (rel. to CMV-*Renilla*) from 293T cells
566 expressing vector, Flag-UFL1, or Flag-RIG-I, followed by mock or SenV infection (18 h) or
567 in B) 293T cells transfected with vector (Vec) or Flag-UFL1, followed by mock or HCV
568 PAMP RNA transfection (24 h). C) RT-qPCR analysis (rel. to *GAPDH*) of RNA extracted
569 from 293T cells transfected vector or Flag-UFL1 that were treated with IFN-β (18 h). D)
570 Immunoblot analysis of p-IRF3 following siRNA transfection along with expression of
571 vector or Flag-UFL1^{siR}, which has point mutations in the siRNA seed sequence.
572 Quantification of p-IRF3/Tubulin is shown on the right. E) RT-qPCR analysis (rel. to *18S*)
573 of RNA extracted from primary neonatal human dermal fibroblasts (NHDFs) transfected
574 with either siCTRL or siUFL1 followed by mock or SenV infection (8 h). F) ELISA for IFN-
575 β of supernatants harvested from NHDFs transfected with siCTRL or siUFL1 and infected
576 with SenV for the indicated times. G) Relative IFN-β-promoter reporter luciferase
577 expression (rel. to CMV-*Renilla*) from 293T cells expressing indicated constructs followed
578 by mock or SenV infection (12-18 h), with results graphed as relative SenV fold change
579 for each. H) Diagram of UFL1 truncation constructs and corresponding ufmylation activity
580 represented as the mean of mock and SenV values normalized to WT. For A) mean -/+
581 SD, n=3 technical replicates and representative of n=3 independent experiments. For all
582 others, mean -/+ SEM, n=3 or n=5 (1G) biological replicates. *$p \leq 0.05$, **$p \leq 0.01$, and
583 ***$p \leq 0.001$ determined by two-way ANOVA followed by Šidák's multiple comparisons
584 test (B, E), Student's t-test (C, D, F), or one-way ANOVA followed by Dunnett's multiple
585 comparisons test (G).

586

587 **Figure 2. The ufmylation machinery proteins positively regulate RIG-I signaling.**

588 A) IFN-β-promoter reporter luciferase expression (rel. to CMV-*Renilla*) from 293T cells
589 expressing vector or Flag-UFM1, followed by mock or SenV infection (18 h) or in B) WT
590 or CRISPR/CAS9 UFM1 KO 293T cells transfected with vector (Vec) or Flag-UFM1 (for
591 KO), followed by mock or SenV infection (18 h). C) ELISA for IFN-β of supernatants
592 harvested from WT or CRISPR/CAS9 UFM1 KO 293T cells that were SenV infected (18
593 h). D) Diagram of UFM1 conjugation. E) Relative IFN-β-promoter reporter luciferase
594 expression (rel. to CMV-*Renilla*) from 293T cells expressing indicated constructs followed
595 by mock or SenV infection (18 h), with results graphed as relative SenV fold change for
596 each. Represented as mean -/+ SEM, n=3 biological replicates. *$p \leq 0.05$, **$p \leq 0.01$, and

597 ***p ≤ 0.001 determined by two-way ANOVA followed by Tukey's multiple comparisons
598 test (A-B), Student's t-test (C), or one-way ANOVA followed by Dunnett's multiple
599 comparisons test (E).
600
601 **Figure 3. UFM1 is required for the RIG-I driven transcriptional response.**
602 RNA-seq analysis WT or UFM1 KO 293T cells following mock or SenV infection (18 h).
603 A) Gene set enrichment analysis of negatively regulated differentially expressed genes in
604 SenV-infected 293T cells represented by normalized enrichment score (UFM1 KO / WT).
605 B) Volcano plot of differentially expressed genes (adj P<0.01) shown in grey, with ISGs
606 shown in red, in SenV-infected 293T cells (UFM1 KO / WT). C) Heatmap of the effect of
607 UFM1 KO on the fold change of the 50 most induced IFN and ISGs (UFM1 KO / WT)
608 following SenV infection (adj P<0.01).
609
610 **Figure 4. UFL1 is recruited to intracellular membranes and interacts with 14-3-3ε**
611 **and RIG-I during RNA virus infection.**
612 A) Immunoblot analysis of inputs and subcellular membrane flotation of 293T cell extracts
613 that were mock or SenV-infected (4 h) followed by sucrose gradient fractionation, with
614 fraction numbers indicated from the top of the gradient (1) to bottom (8). Fractionation
615 controls, GAPDH for cytosol and Cox-I for membranes, are indicated and reveal that the
616 membranes are localized to fraction #1. Relative quantification of the ratio of UFL1 to a
617 membrane marker (Cox-I) in fraction 1 normalized to total protein levels in inputs are
618 shown on the right. B) Immunoblot analysis of anti-Flag immunoprecipitated extracts and
619 inputs from 293T cells expressing Myc-14-3-3ε and Flag-UFL1 that were mock- or SenV-
620 infected (4 h), with relative quantification on right. C) Immunoblot analysis of anti-Flag
621 immunoprecipitated extracts and inputs from 293T cells expressing Myc-UFL1 and Flag-
622 RIG-I that were mock- or SenV-infected (4 h), with relative quantification with IP values
623 normalized to inputs values on right. D) Immunoblot analysis of anti-RIG-I
624 immunoprecipitated (or anti-IgG) extracts and inputs from 293T cells that were mock- or
625 SenV-infected (4 h), with relative quantification with IP values normalized to inputs values
626 on right. E) Immunoblot analysis of anti-Flag immunoprecipitated extracts and inputs from
627 293T cells expressing Myc-UFL1 and Flag-RIG-I constructs that were mock- or SenV-
628 infected (4 h), with results quantified as relative fold change (SenV to Mock) for each. The
629 graphs are represented as the mean -/+ SEM, n=3 (A-B, D-E) or n=4 (C) biological

630 replicates and *p ≤ 0.05, **p ≤ 0.01, and ***p ≤ 0.001 determined by Student's t-test (A-D)
631 or one-way ANOVA followed by Dunnett's multiple comparisons test (E).
632
633 **Figure 5. UFL1 interaction with RIG-I requires 14-3-3ε and ufmylation.**
634 A) Immunoblot analysis of anti-HA immunoprecipitated extracts and inputs from 293T cells
635 transfected with siCTRL or si14-3-3ε followed by SenV infection (4h). B) Immunoblot of
636 anti-HA immunoprecipitated extracts and inputs from 293T WT or UFM1 KO cells
637 transfected with HA-RIG-I and Flag-UFL1. C) Immunoblot of anti-Flag immunoprecipitated
638 extracts and inputs from 293T WT or UFM1 KO cells transfected with Flag-UFL1 and Myc-
639 14-3-3ε. In (A-C), SenV infection was for 4 hours, and relative quantification is shown on
640 the right, indicating the mean -/+ SEM (A, B), n=3 (A, B) biological replicates. For (C)
641 values shown are SD of IP values adjusted for input expression, with n=2 biological
642 replicates. *p ≤ 0.05, **p ≤ 0.01, and ***p ≤ 0.001 determined by Student's t-test.
643
644 **Figure 6. Ufmylation promotes RIG-I interaction with 14-3-3ε for MAVS activation.**
645 A) Immunoblot of anti-Flag immunoprecipitated extracts and inputs from 293T cells
646 transfected with siCTRL or siUFL1 and indicated constructs. B) Immunoblot of anti-Flag
647 immunoprecipitated extracts and inputs from 293T WT or UFM1 KO cells. C) Immunoblot
648 of anti-Myc immunoprecipitated extracts from 293T WT or UFM1 KO cells. D) 293T WT or
649 UFM1 KO were mock or SenV-infected (12 h). Immunoblotting shows endogenous MAVS
650 in input samples and MAVS aggregation from P5 fractions, in the presence or absence of
651 denaturing reagent (β-mercaptoethanol). SenV infection was for 4 h (A-C) or 12 h (D). In
652 (A-C), relative quantification of indicated protein in the IP is shown on the right; in (D) SDD-
653 AGE MAVS values are normalized to corresponding SDS-PAGE values. Graphs show the
654 mean -/+ SEM for n=3 biological replicates. *p ≤ 0.05, **p ≤ 0.01, and ***p ≤ 0.001
655 determined by Student's t-test.
656
657 **Figure S1. The domains of UFL1 that form UFM1 conjugates in cells.**
658 Quantification of immunoblots from 293T cells expressing indicated Flag-UFL1
659 constructs or vector followed by mock or SenV infection (18 h) represented as the ratio
660 of UFM1 conjugates (approximately 25-50 kDa) to Flag-UFL1 expression in each lane

661 normalized to loading control with WT Flag-UFL1 mock set to 100. Graph indicates the
662 mean -/+ SEM for n=3 biological replicates.
663
664 **Fig. S2. Transcriptional response of genes negatively regulated by UFM1.**
665 RNA-seq analysis of WT versus UFM1 KO 293T cells showing the gene set enrichment
666 analysis (top 10 categories) of negatively regulated differentially expressed genes
667 represented by normalized enrichment score to identify gene ontology terms and
668 pathways associated with altered gene expression for each of the comparisons
669 performed (adj P<0.01).
670
671 **Dataset S1.** Differential expression analysis from RNA-seq analysis for UFM1 KO / WT
672 293T cells
673 Table S1.1: UFM1 KO / WT Mock
674 Table S1.2 UFM1 KO / WT SenV (18 h)
675
676 **Dataset S2.** Gene Set Enrichment Analysis for UFM1 KO / WT 293T cells
677 Table S2.1: UFM1 KO / WT Mock- negative direction
678 Table S2.2 UFM1 KO / WT SenV (18 h)- negative direction
679 Table S2.3 UFM1 KO / WT Mock- positive direction
680 Table S2.4 UFM1 KO / WT SenV (18 h)- negative direction

681 **References**

682

683 1. D. Thoresen, *et al.*, The molecular mechanism of RIG-I activation and signaling. *Immunol*
684 *Rev* (2021) https:/doi.org/10.1111/imr.13022.

685 2. M. J. McFadden, N. S. Gokhale, S. M. Horner, Protect this house: cytosolic sensing of
686 viruses. *Current Opinion in Virology* **22**, 36–43 (2017).

687 3. J. Rehwinkel, M. U. Gack, RIG-I-like receptors: their regulation and roles in RNA sensing.
688 *Nature Reviews Immunology*, 1–15 (2020).

689 4. C. Chiang, M. U. Gack, Post-translational Control of Intracellular Pathogen Sensing
690 Pathways. *Trends in Immunology* **38**, 39–52 (2017).

691 5. M. U. Gack, *et al.*, TRIM25 RING-finger E3 ubiquitin ligase is essential for RIG-I-mediated
692 antiviral activity. *Nature* **446**, 916–920 (2007).

693 6. H. Oshiumi, M. Matsumoto, S. Hatakeyama, T. Seya, Riplet/RNF135, a RING finger
694 protein, ubiquitinates RIG-I to promote interferon-beta induction during the early phase of
695 viral infection. *J. Biol. Chem.* **284**, 807–817 (2009).

696 7. H. M. Liu, *et al.*, The Mitochondrial Targeting Chaperone 14-3-3ε Regulates a RIG-I
697 Translocon that Mediates Membrane Association and Innate Antiviral Immunity. *Cell Host*
698 *& Microbe* **11**, 528–537 (2012).

699 8. H. Oshiumi, Recent Advances and Contradictions in the Study of the Individual Roles of
700 Ubiquitin Ligases That Regulate RIG-I-Like Receptor-Mediated Antiviral Innate Immune
701 Responses. *Front Immunol* **11**, 1296 (2020).

702 9. Y. K. Chan, M. U. Gack, A phosphomimetic-based mechanism of dengue virus to
703 antagonize innate immunity. *Nature Immunology* **17**, 523–530 (2016).

704 10. W. Riedl, *et al.*, Zika Virus NS3 Mimics a Cellular 14-3-3-Binding Motif to Antagonize RIG-
705 I- and MDA5-Mediated Innate Immunity. *Cell Host & Microbe* **26**, 493-503.e6 (2019).

706 11. C. Vazquez, S. M. Horner, MAVS Coordination of Antiviral Innate Immunity. *J Virol* **89**,
707 6974–6977 (2015).

708 12. E.-H. Tam, *et al.*, Role of the chaperone protein 14-3-3ε in the regulation of influenza A
709 virus-activated beta interferon. *J Virol*, JVI0023121 (2021).

710 13. S. M. Horner, H. M. Liu, H. S. Park, J. Briley, M. Gale, Mitochondrial-associated
711 endoplasmic reticulum membranes (MAM) form innate immune synapses and are targeted
712 by hepatitis C virus. *Proc Natl Acad Sci U S A* **108**, 14590–14595 (2011).

713 14. S. M. Horner, C. Wilkins, S. Badil, J. Iskarpatyoti, M. G. Jr, Proteomic Analysis of
714 Mitochondrial-Associated ER Membranes (MAM) during RNA Virus Infection Reveals
715 Dynamic Changes in Protein and Organelle Trafficking. *PLOS ONE* **10**, e0117963 (2015).

716 15. D. C. Beachboard, *et al.*, The small GTPase RAB1B promotes antiviral innate immunity by
717 interacting with TNF receptor–associated factor 3 (TRAF3). *J. Biol. Chem.*,
718 jbc.RA119.007917 (2019).

719 16. K. Tatsumi, *et al.*, A novel type of E3 ligase for the Ufm1 conjugation system. *J. Biol.*
720 *Chem.* **285**, 5417–5427 (2010).

721 17. M. Komatsu, *et al.*, A novel protein-conjugating system for Ufm1, a ubiquitin-fold modifier.
722 *EMBO J* **23**, 1977–1986 (2004).

723 18. S. H. Kang, *et al.*, Two novel ubiquitin-fold modifier 1 (Ufm1)-specific proteases, UfSP1
724 and UfSP2. *J. Biol. Chem.* **282**, 5256–5262 (2007).

725 19. Y. Wei, X. Xu, UFMylation: A Unique & Fashionable Modification for Life. *Genomics*
726 *Proteomics Bioinformatics* **14**, 140–146 (2016).

727 20. J. Daniel, E. Liebau, The Ufm1 Cascade. *Cells* **3**, 627–638 (2014).

728 21. L. Wang, *et al.*, UFMylation of RPL26 links translocation-associated quality control to
729 endoplasmic reticulum protein homeostasis. *Cell Res*, 1–16 (2019).

730 22. Z. Wang, *et al.*, MRE11 UFMylation promotes ATM activation. *Nucleic Acids Research* **47**,
731 4124–4135 (2019).

732 23. H. M. Yoo, *et al.*, Modification of ASC1 by UFM1 is crucial for ERα transactivation and
733 breast cancer development. *Mol. Cell* **56**, 261–274 (2014).

734 24. B. Qin, *et al.*, UFL1 promotes histone H4 ufmylation and ATM activation. *Nat Commun* **10**,
735 1242 (2019).

736 25. I. A. Gak, *et al.*, UFMylation regulates translational homeostasis and cell cycle progression.
737 *bioRxiv*, 2020.02.03.931196 (2020).

738 26. R. DeJesus, *et al.*, Functional CRISPR screening identifies the ufmylation pathway as a
739 regulator of SQSTM1/p62. *eLife* **5**, e17290 (2016).

740 27. J. R. Liang, *et al.*, A Genome-wide ER-phagy Screen Highlights Key Roles of Mitochondrial
741 Metabolism and ER-Resident UFMylation. *Cell* **0** (2020).

742 28. C. P. Walczak, *et al.*, Ribosomal protein RPL26 is the principal target of UFMylation. *PNAS*
743 **116**, 1299–1308 (2019).

744 29. Y. Cai, N. Singh, H. Li, Essential role of Ufm1 conjugation in the hematopoietic system.
745 *Exp. Hematol.* **44**, 442–446 (2016).

746 30. J. Kulsuptrakul, R. Wang, N. L. Meyers, M. Ott, A. S. Puschnik, A genome-wide CRISPR
747 screen identifies UFMylation and TRAMP-like complexes as host factors required for
748 hepatitis A virus infection. *Cell Reports* **34** (2021).

749 31. D. R. Balce, *et al.*, UFMylation inhibits the proinflammatory capacity of interferon-γ–
750 activated macrophages. *PNAS* **118** (2021).

751 32. Y.-M. Loo, *et al.*, Viral and therapeutic control of IFN-β promoter stimulator 1 during
752 hepatitis C virus infection. *PNAS* **103**, 6001–6006 (2006).

753 33. R. Sumpter, *et al.*, Regulating intracellular antiviral defense and permissiveness to
754 hepatitis C virus RNA replication through a cellular RNA helicase, RIG-I. *J Virol* **79**, 2689–
755 2699 (2005).

756 34. T. Saito, D. M. Owen, F. Jiang, J. Marcotrigiano, M. Gale, Innate immunity induced by
757 composition-dependent RIG-I recognition of hepatitis C virus RNA. *Nature* **454**, 523–527
758 (2008).

759 35. D. Simsek, *et al.*, The Mammalian Ribo-interactome Reveals Ribosome Functional
760 Diversity and Heterogeneity. *Cell* **169**, 1051-1065.e18 (2017).

761 36. M. J. McFadden, *et al.*, Post-transcriptional regulation of antiviral gene expression by N6-
762 methyladenosine. *Cell Reports* **34**, 108798 (2021).

763 37. A. Peisley, B. Wu, H. Xu, Z. J. Chen, S. Hur, Structural basis for ubiquitin-mediated
764 antiviral signal activation by RIG-I. *Nature* **509**, 110–114 (2014).

765 38. A. Mizutani, M. Fukuda, K. Ibata, Y. Shiraishi, K. Mikoshiba, SYNCRIP, a Cytoplasmic
766 Counterpart of Heterogeneous Nuclear Ribonucleoprotein R, Interacts with Ubiquitous
767 Synaptotagmin Isoforms*. *Journal of Biological Chemistry* **275**, 9823–9831 (2000).

768 39. E. Foy, *et al.*, Control of antiviral defenses through hepatitis C virus disruption of retinoic
769 acid-inducible gene-I signaling. *Proc. Natl. Acad. Sci. U.S.A.* **102**, 2986–2991 (2005).

770 40. E. Meylan, *et al.*, Cardif is an adaptor protein in the RIG-I antiviral pathway and is targeted
771 by hepatitis C virus. *Nature* **437**, 1167–1172 (2005).

772 41. X.-D. Li, L. Sun, R. B. Seth, G. Pineda, Z. J. Chen, Hepatitis C virus protease NS3/4A
773 cleaves mitochondrial antiviral signaling protein off the mitochondria to evade innate
774 immunity. *Proc Natl Acad Sci U S A* **102**, 17717–17722 (2005).

775 42. R. Lin, *et al.*, Dissociation of a MAVS/IPS-1/VISA/Cardif-IKKepsilon molecular complex
776 from the mitochondrial outer membrane by hepatitis C virus NS3-4A proteolytic cleavage. *J*
777 *Virol* **80**, 6072–6083 (2006).

778 43. K. Takahasi, *et al.*, Nonself RNA-Sensing Mechanism of RIG-I Helicase and Activation of
779 Antiviral Immune Responses. *Molecular Cell* **29**, 428–440 (2008).

780 44. H. Oshiumi, M. Miyashita, M. Matsumoto, T. Seya, A distinct role of Riplet-mediated K63-
781 Linked polyubiquitination of the RIG-I repressor domain in human antiviral innate immune
782 responses. *PLoS Pathog.* **9**, e1003533 (2013).

783 45. F. Hou, *et al.*, MAVS Forms Functional Prion-like Aggregates to Activate and Propagate
784 Antiviral Innate Immune Response. *Cell* **146**, 448–461 (2011).

785 46. N. Zamorano Cuervo, Q. Osseman, N. Grandvaux, Virus Infection Triggers MAVS
786 Polymers of Distinct Molecular Weight. *Viruses* **10** (2018).

787 47. W. Zeng, *et al.*, Reconstitution of the RIG-I pathway reveals a signaling role of unanchored
788 polyubiquitin chains in innate immunity. *Cell* **141**, 315–330 (2010).

789 48. X. Jiang, *et al.*, Ubiquitin-induced oligomerization of the RNA sensors RIG-I and MDA5
790 activates antiviral innate immune response. *Immunity* **36**, 959–973 (2012).

791 49. L. Wang, *et al.*, UFMylation of RPL26 links translocation-associated quality control to
792 endoplasmic reticulum protein homeostasis. *Cell Research* **30**, 5–20 (2020).

793 50. Y. Zhang, M. Zhang, J. Wu, G. Lei, H. Li, Transcriptional regulation of the Ufm1
794 conjugation system in response to disturbance of the endoplasmic reticulum homeostasis
795 and inhibition of vesicle trafficking. *PLoS ONE* **7**, e48587 (2012).

796 51. C. Kwak, *et al.*, Contact-ID, a tool for profiling organelle contact sites, reveals regulatory
797 proteins of mitochondrial-associated membrane formation. *PNAS* **117**, 12109–12120
798 (2020).

799 52. Y. Merbl, P. Refour, H. Patel, M. Springer, M. W. Kirschner, Profiling of ubiquitin-like
800 modifications reveals features of mitotic control. *Cell* **152**, 1160–1172 (2013).

801 53. L. Wang, *et al.*, UFMylation of RPL26 links translocation-associated quality control to
802 endoplasmic reticulum protein homeostasis. *Cell Res.* **30**, 5–20 (2020).

803 54. M. Hochstrasser, Origin and function of ubiquitin-like proteins. *Nature* **458**, 422–429
804 (2009).

805 55. K. N. Swatek, D. Komander, Ubiquitin modifications. *Cell Research* **26**, 399–422 (2016).

806 56. A. J. Muslin, J. W. Tanner, P. M. Allen, A. S. Shaw, Interaction of 14-3-3 with Signaling
807 Proteins Is Mediated by the Recognition of Phosphoserine. *Cell* **84**, 889–897 (1996).

808 57. Y. Aghazadeh, V. Papadopoulos, The role of the 14-3-3 protein family in health, disease,
809 and drug development. *Drug Discovery Today* **21**, 278–287 (2016).

810 58. A. Aitken, Post-translational modification of 14-3-3 isoforms and regulation of cellular
811 function. *Seminars in Cell & Developmental Biology* **22**, 673–680 (2011).

812 59. J.-P. Lin, Y.-K. Fan, H. M. Liu, The 14-3-3η chaperone protein promotes antiviral innate
813 immunity via facilitating MDA5 oligomerization and intracellular redistribution. *PLoS*
814 *Pathog.* **15**, e1007582 (2019).

815 60. K. Onomoto, K. Onoguchi, M. Yoneyama, Regulation of RIG-I-like receptor-mediated
816 signaling: interaction between host and viral factors. *Cell Mol Immunol* **18**, 539–555 (2021).

817 61. G. Liu, *et al.*, ISG15-dependent activation of the sensor MDA5 is antagonized by the
818 SARS-CoV-2 papain-like protease to evade host innate immunity. *Nature Microbiology*, 1–
819 12 (2021).

820 62. M. Yoneyama, *et al.*, Shared and Unique Functions of the DExD/H-Box Helicases RIG-I,
821 MDA5, and LGP2 in Antiviral Innate Immunity. *The Journal of Immunology* **175**, 2851–
822 2858 (2005).

823 63. B. Fredericksen, *et al.*, Activation of the Interferon-β Promoter During Hepatitis C Virus
824 RNA Replication. *Viral Immunology* **15**, 29–40 (2002).

825 64. T. Saito, *et al.*, Regulation of innate antiviral defenses through a shared repressor domain
826 in RIG-I and LGP2. *PNAS* **104**, 582–587 (2007).

827 65. F. A. Ran, *et al.*, Genome engineering using the CRISPR-Cas9 system. *Nat Protoc* **8**,
828 2281–2308 (2013).

829 66. Babraham Bioinformatics - Trim Galore! (October 12, 2021).

830 67. M. Martin, Cutadapt removes adapter sequences from high-throughput sequencing reads.
831 *EMBnet.journal* **17**, 10–12 (2011).

832 68. P. J. Kersey, *et al.*, Ensembl Genomes: an integrative resource for genome-scale data
833 from non-vertebrate species. *Nucleic Acids Res* **40**, D91-97 (2012).

834 69. A. Dobin, *et al.*, STAR: ultrafast universal RNA-seq aligner. *Bioinformatics* **29**, 15–21
835 (2013).

836 70. HTSeq: Analysing high-throughput sequencing data with Python — HTSeq 0.13.5
837 documentation (October 12, 2021).

838 71. M. I. Love, W. Huber, S. Anders, Moderated estimation of fold change and dispersion for
839 RNA-seq data with DESeq2. *Genome Biology* **15**, 550 (2014).

840 72. W. Huber, *et al.*, Orchestrating high-throughput genomic analysis with Bioconductor. *Nat*
841 *Methods* **12**, 115–121 (2015).

842 73. V. K. Mootha, *et al.*, PGC-1alpha-responsive genes involved in oxidative phosphorylation
843 are coordinately downregulated in human diabetes. *Nat Genet* **34**, 267–273 (2003).

844 74. H. M. Liu, *et al.*, SYNCRIP (synaptotagmin-binding, cytoplasmic RNA-interacting protein) is
845 a host factor involved in hepatitis C virus RNA replication. *Virology* **386**, 249–256 (2009).

846

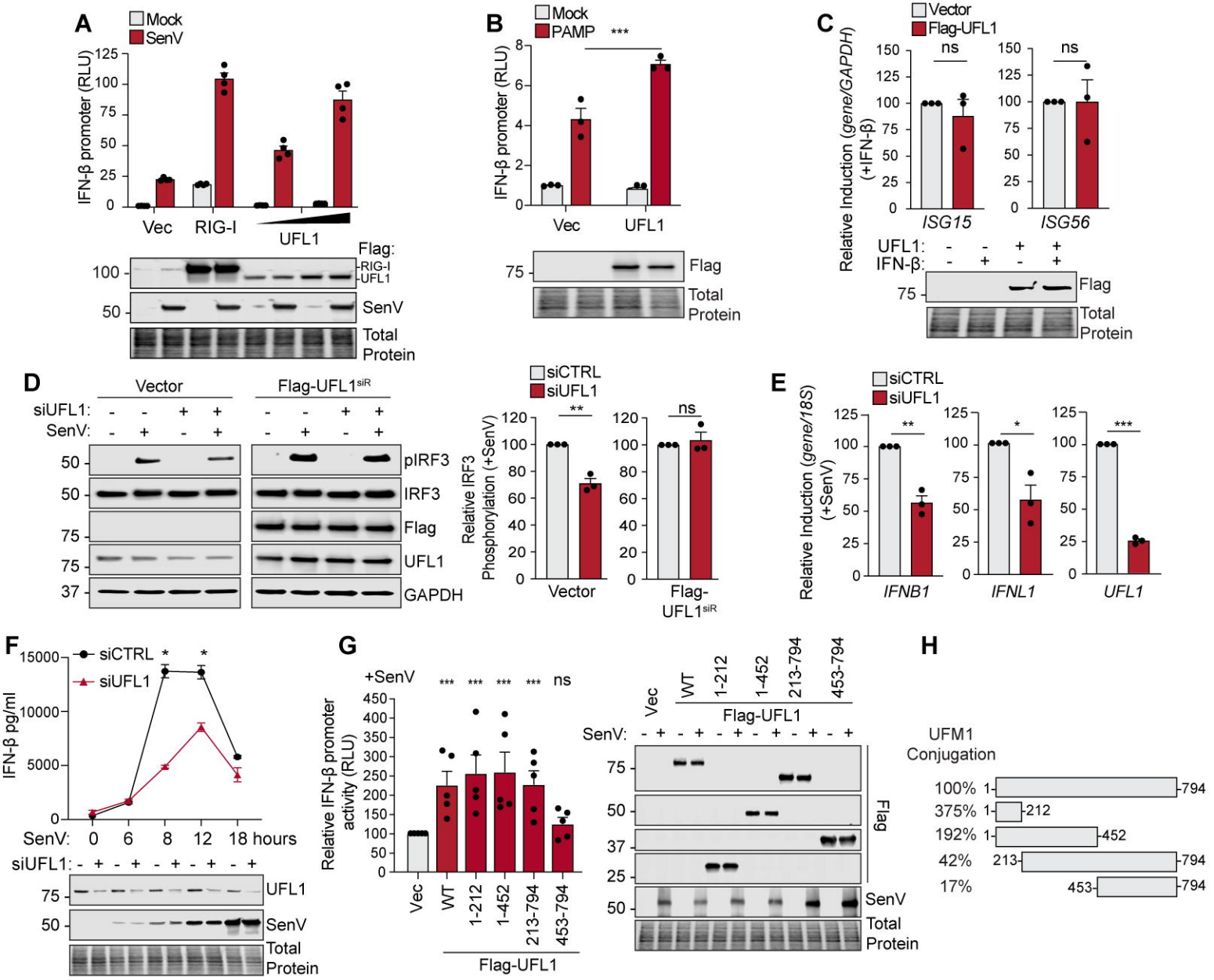
A
Mock
SenV
IFN-β promoter (RLU)
Vec
RIG-I
UFL1
Flag:
RIG-I
UFL1
SenV
Total Protein
B
Mock
PAMP
***
IFN-β promoter (RLU)
Vec
UFL1
Flag
Total Protein
C
Vector
Flag-UFL1
ns
Relative Induction (gene/GAPDH) (+IFN-β)
ISG15
ISG56
UFL1:
IFN-β:
Flag
Total Protein
D
Vector
Flag-UFL1siR
siUFL1:
SenV:
pIRF3
IRF3
Flag
UFL1
GAPDH
siCTRL
siUFL1
Relative IRF3 Phosphorylation (+SenV)
Vector
Flag-UFL1siR
E
siCTRL
siUFL1
Relative Induction (gene/18S) (+SenV)
IFNB1
IFNL1
UFL1
F
siCTRL
siUFL1
IFN-β pg/ml
SenV: 0 6 8 12 18 hours
siUFL1:
UFL1
SenV
Total Protein
G
+SenV
Relative IFN-β promoter activity (RLU)
Vec
WT
1-212
1-452
213-794
453-794
Flag-UFL1
SenV:
Flag
SenV
Total Protein
H
UFM1 Conjugation
100% 1-794
375% 1-212
192% 1-452
42% 213-794
17% 453-794

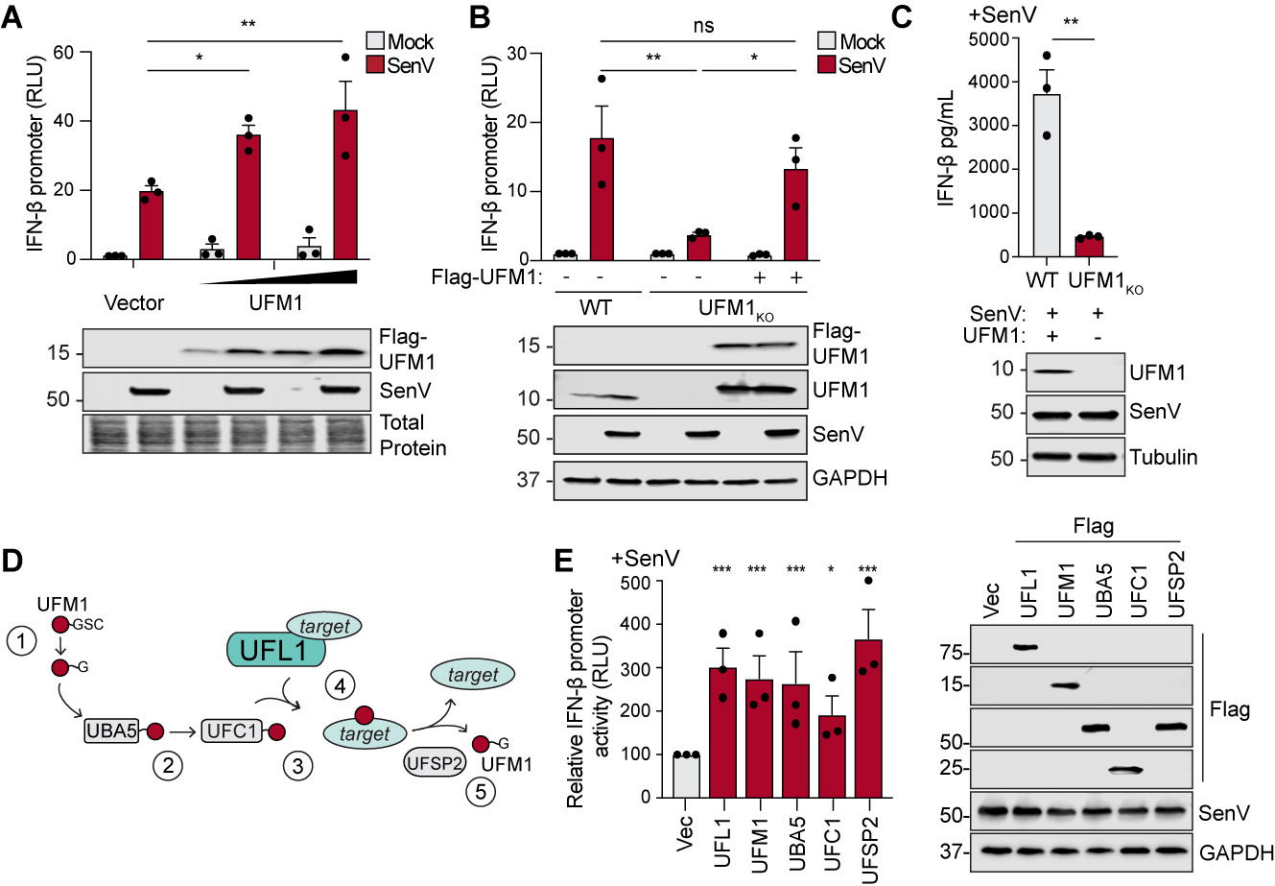
A
Mock
SenV
IFN-β promoter (RLU)
Vector
UFM1
Flag-UFM1
SenV
Total Protein
B
ns
Flag-UFM1:
WT
UFM1KO
Flag-UFM1
UFM1
SenV
GAPDH
C
+SenV
IFN-β pg/mL
SenV:
UFM1:
Tubulin
D
UFM1
GSC
G
UBA5
UFC1
UFL1
target
UFSP2
E
+SenV
Relative IFN-β promoter activity (RLU)
Vec
UFL1
UFM1
UBA5
UFC1
UFSP2
Flag
SenV
GAPDH

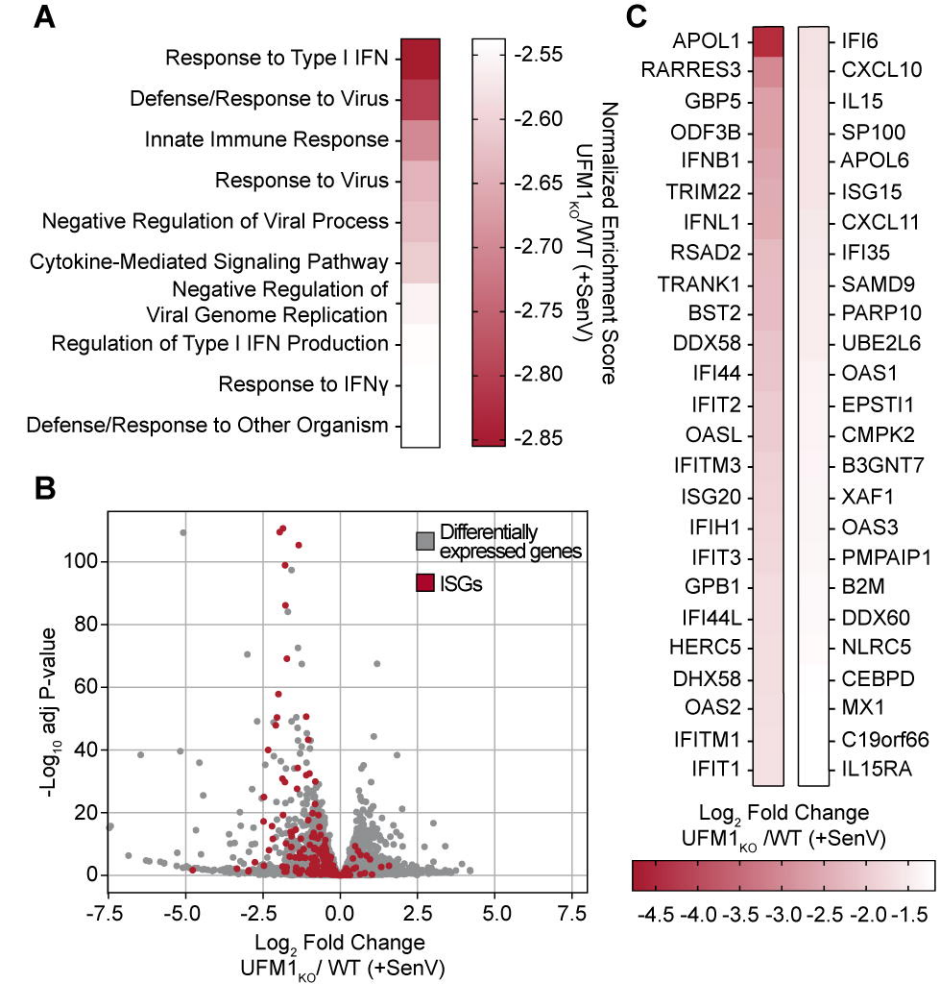
A
Response to Type I IFN
Defense/Response to Virus
Innate Immune Response
Response to Virus
Negative Regulation of Viral Process
Cytokine-Mediated Signaling Pathway
Negative Regulation of Viral Genome Replication
Regulation of Type I IFN Production
Response to IFNγ
Defense/Response to Other Organism
-2.55
-2.60
-2.65
-2.70
-2.75
-2.80
-2.85
Normalized Enrichment Score
UFM1KO/WT (+SenV)
B
Differentially expressed genes
ISGs
-Log10 adj P-value
100
80
60
40
20
0
-7.5
-5.0
-2.5
0.0
2.5
5.0
7.5
Log2 Fold Change
UFM1KO/ WT (+SenV)
C
APOL1
RARRES3
GBP5
ODF3B
IFNB1
TRIM22
IFNL1
RSAD2
TRANK1
BST2
DDX58
IFI44
IFIT2
OASL
IFITM3
ISG20
IFIH1
IFIT3
GPB1
IFI44L
HERC5
DHX58
OAS2
IFITM1
IFIT1
IFI6
CXCL10
IL15
SP100
APOL6
ISG15
CXCL11
IFI35
SAMD9
PARP10
UBE2L6
OAS1
EPSTI1
CMPK2
B3GNT7
XAF1
OAS3
PMPAIP1
B2M
DDX60
NLRC5
CEBPD
MX1
C19orf66
IL15RA
Log2 Fold Change
UFM1KO /WT (+SenV)
-4.5 -4.0 -3.5 -3.0 -2.5 -2.0 -1.5

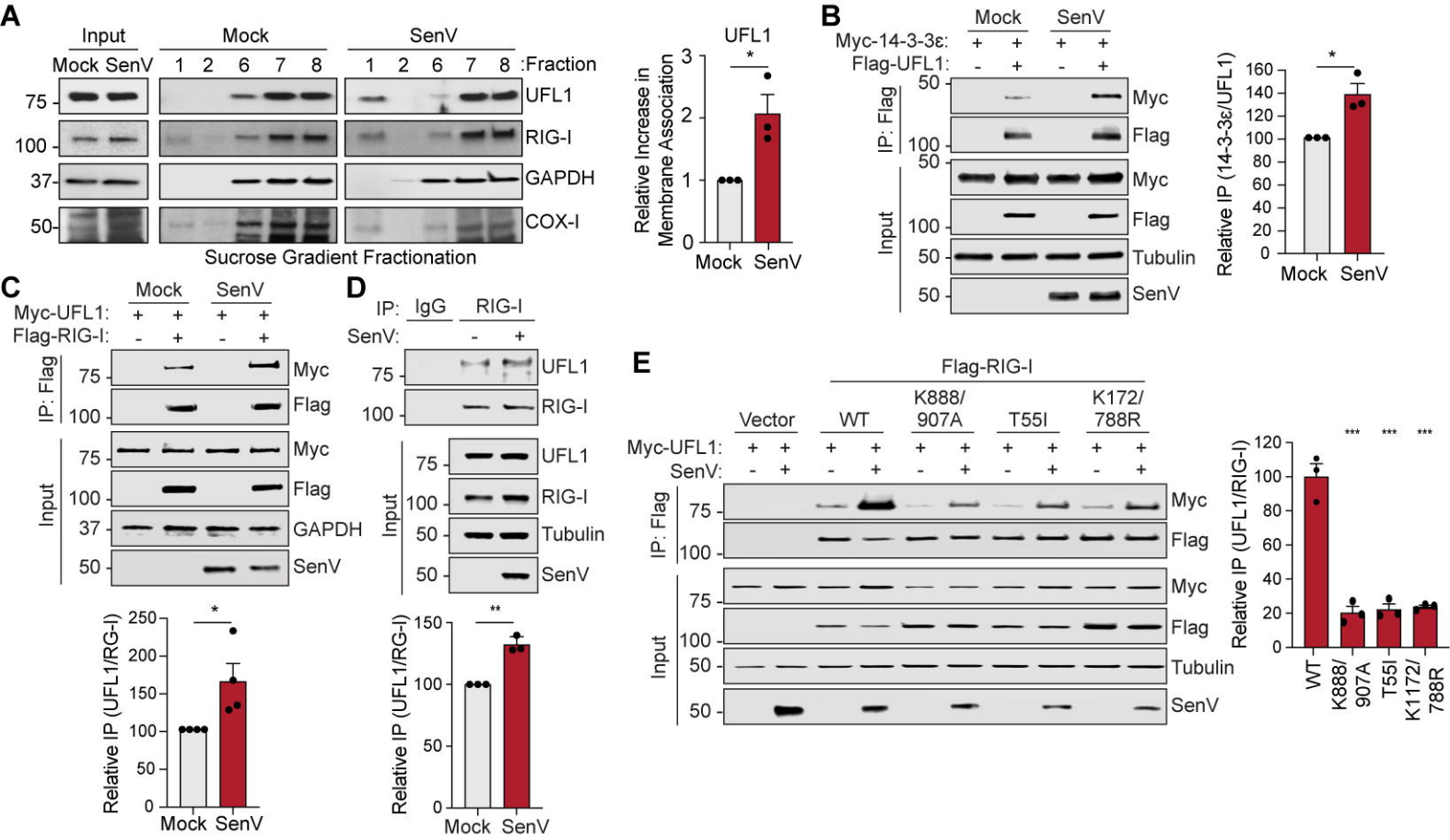
A
Input
Mock
SenV
Mock SenV
1 2 6 7 8
1 2 6 7 8 :Fraction
75
100
37
50
UFL1
RIG-I
GAPDH
COX-I
Sucrose Gradient Fractionation
UFL1
Relative Increase in Membrane Association
Mock SenV
B
Mock
SenV
Myc-14-3-3ε:
Flag-UFL1:
IP: Flag
Input
Myc
Flag
Tubulin
SenV
Relative IP (14-3-3ε/UFL1)
Mock SenV
C
Mock
SenV
Myc-UFL1:
Flag-RIG-I:
IP: Flag
Input
Myc
Flag
GAPDH
SenV
Relative IP (UFL1/RG-I)
Mock SenV
D
IP: IgG RIG-I
SenV:
UFL1
RIG-I
Input
Tubulin
SenV
Relative IP (UFL1/RG-I)
Mock SenV
E
Flag-RIG-I
Vector
WT
K888/ 907A
T55I
K172/ 788R
Myc-UFL1:
SenV:
IP: Flag
Input
Myc
Flag
Tubulin
SenV
Relative IP (UFL1/RIG-I)
WT
K888/ 907A
T55I
K1172/ 788R

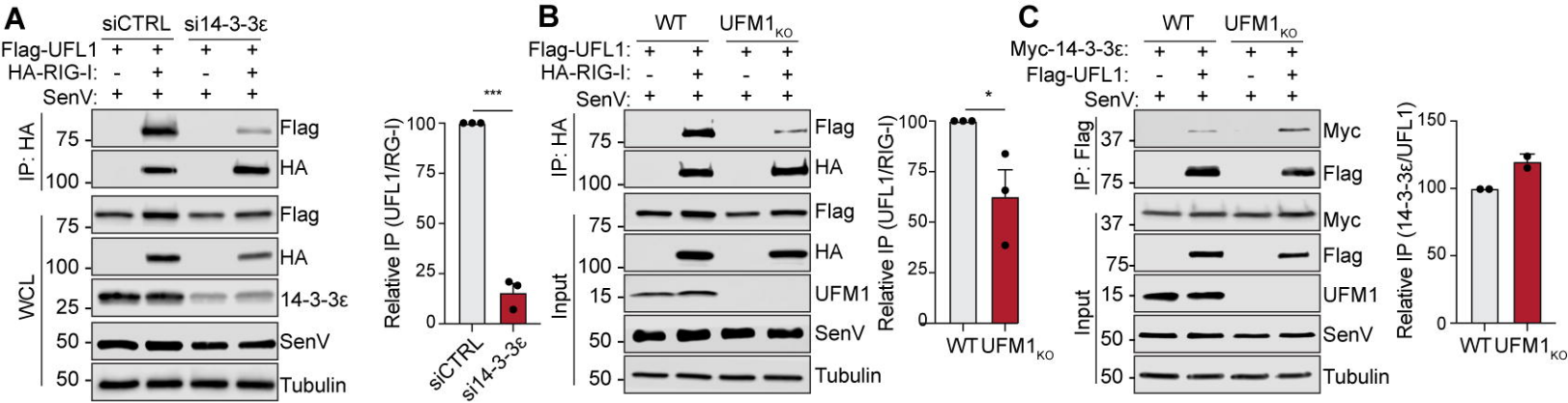
A
siCTRL
si14-3-3ε
Flag-UFL1
HA-RIG-I:
SenV:
IP: HA
WCL
Flag
HA
14-3-3ε
SenV
Tubulin
Relative IP (UFL1/RG-I)
siCTRL
si14-3-3ε
B
WT
UFM1KO
Flag-UFL1:
HA-RIG-I:
SenV:
IP: HA
Input
UFM1
Relative IP (UFL1/RIG-I)
C
Myc-14-3-3ε:
Flag-UFL1:
IP: Flag
Myc
Relative IP (14-3-3ε/UFL1)

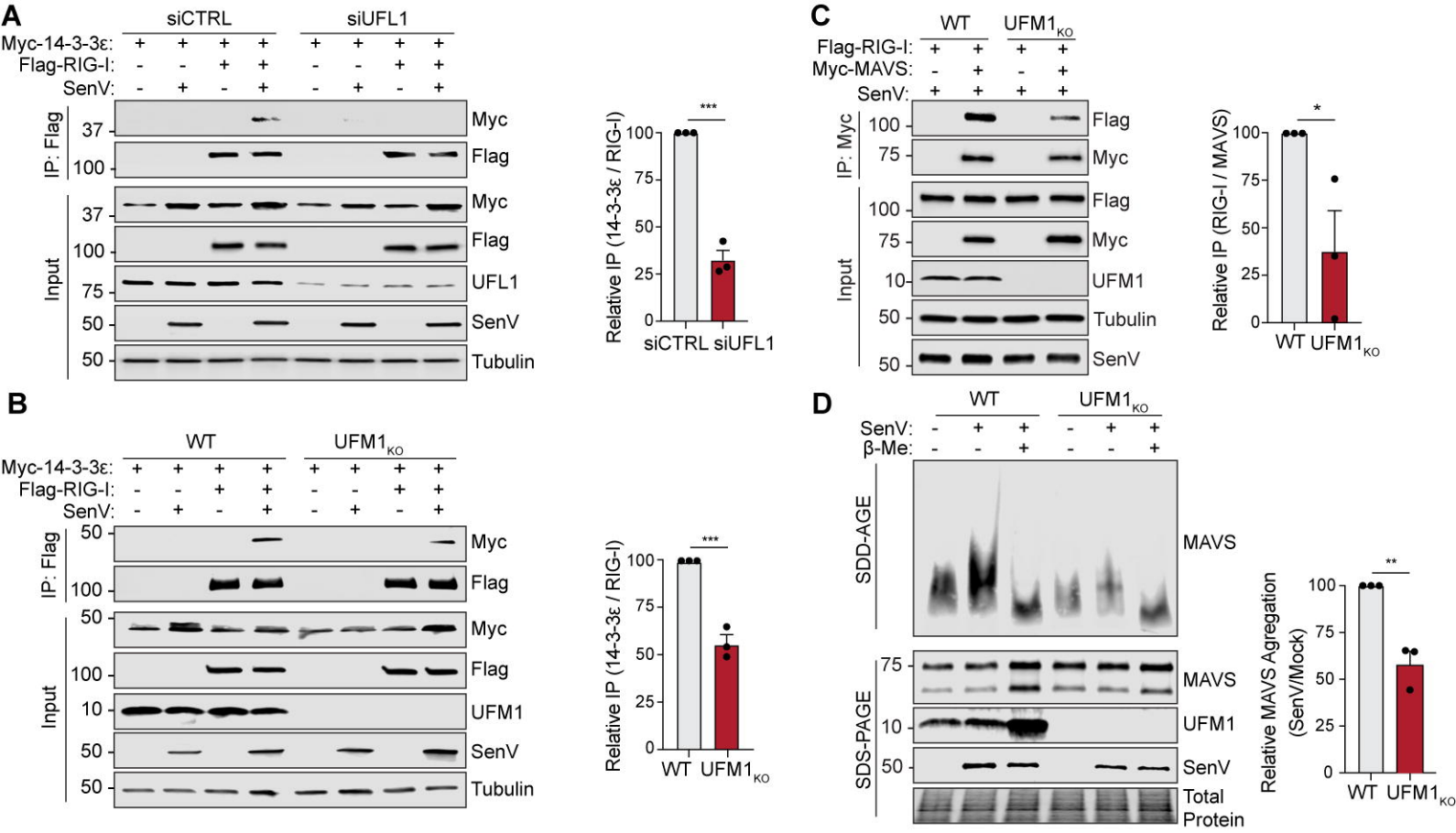
A
siCTRL
siUFL1
Myc-14-3-3ε:
Flag-RIG-I:
SenV:
IP: Flag
Input
Myc
Flag
UFL1
SenV
Tubulin
Relative IP (14-3-3ε / RIG-I)
siCTRL siUFL1
B
WT
UFM1KO
UFM1
C
Flag-RIG-I:
Myc-MAVS:
SenV:
Relative IP (RIG-I / MAVS)
D
SenV:
β-Me:
SDD-AGE
SDS-PAGE
MAVS
Total Protein
Relative MAVS Agregation (SenV/Mock)

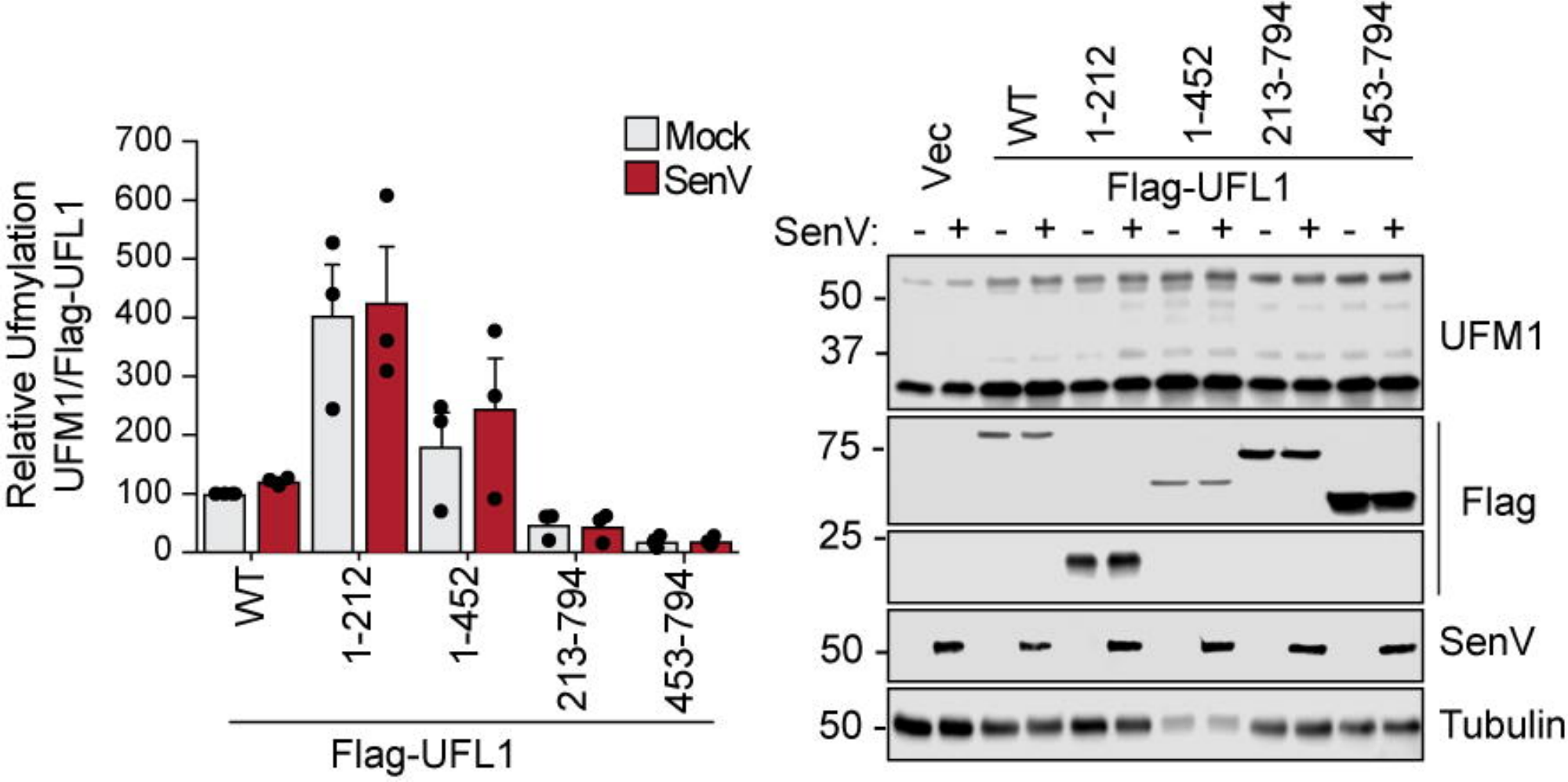
Relative Ufmylation
UFM1/Flag-UFL1
700
600
500
400
300
200
100
0
Mock
SenV
WT
1-212
1-452
213-794
453-794
Flag-UFL1
Vec
WT
1-212
1-452
213-794
453-794
Flag-UFL1
SenV: - + - + - + - + - + - +
50
37
UFM1
75
25
Flag
50
SenV
50
Tubulin

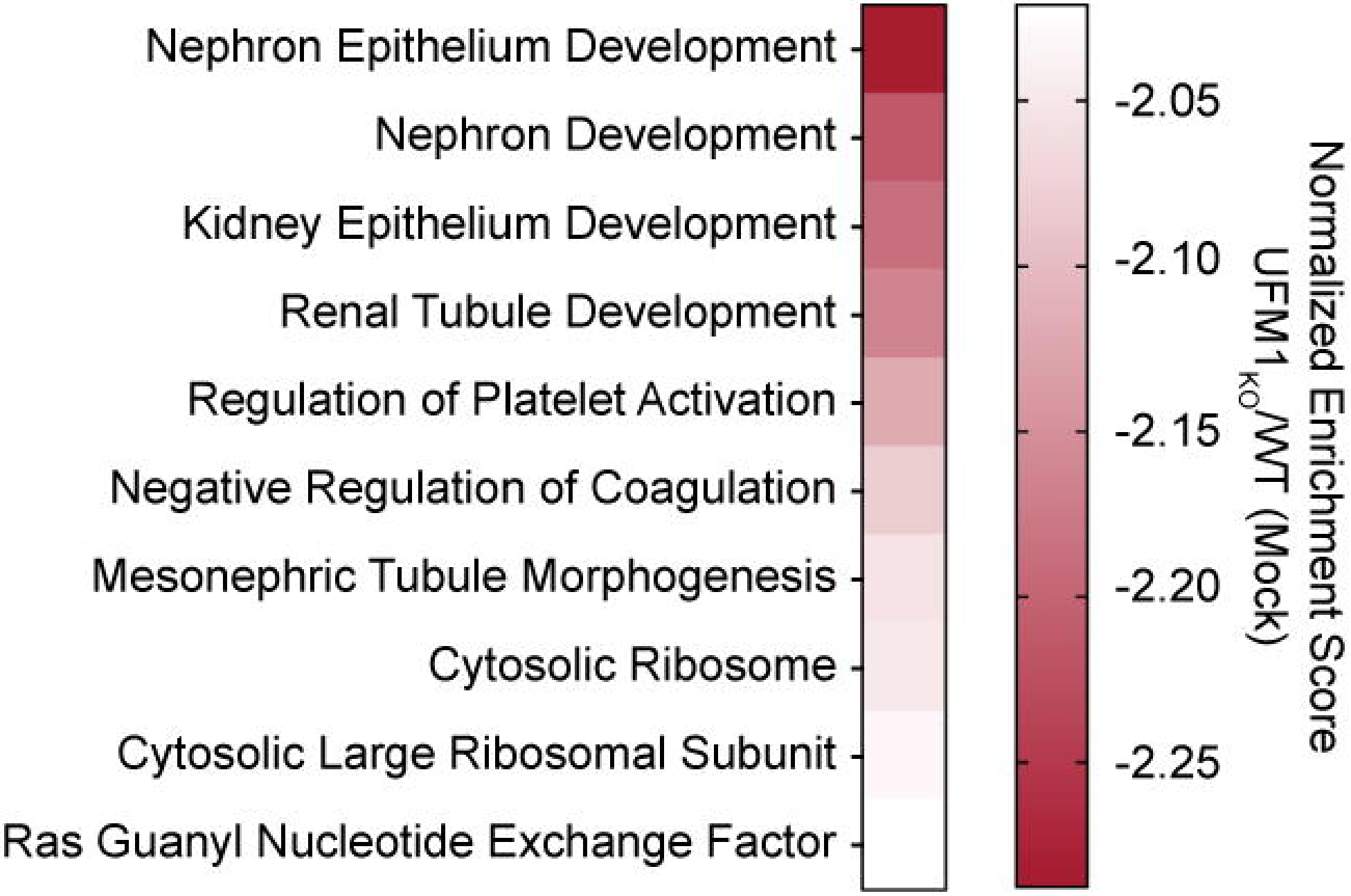
Nephron Epithelium Development
Nephron Development
Kidney Epithelium Development
Renal Tubule Development
Regulation of Platelet Activation
Negative Regulation of Coagulation
Mesonephric Tubule Morphogenesis
Cytosolic Ribosome
Cytosolic Large Ribosomal Subunit
Ras Guanyl Nucleotide Exchange Factor
-2.05
-2.10
-2.15
-2.20
-2.25
Normalized Enrichment Score
UFM1KO/WT (Mock)